Comparative studies of multiwalled carbon nanotube sheets before and after shrinking

Yang Wei, Kaili Jiang,* Xiaofeng Feng, Peng Liu, Liang Liu,† and Shoushan Fan
Department of Physics and Tsinghua-Foxconn Nanotechnology Research Center, Tsinghua University, Beijing 100084, People's Republic of China

(Received 24 January 2007; revised manuscript received 27 April 2007; published 25 July 2007)

The multiwalled carbon nanotube (MWCNT) yarns converted from superaligned MWCNT arrays are self-assembled sheetlike structure in which MWCNTs are aligned along the stretching direction and will shrink into a tight fiber after passing through volatile solvents. In this paper, we report the comparative studies on the physical properties of the MWCNT sheets and shrunk yarns. The major differences between them lie in the surface area and intertube interactions, which result in different mechanical and electrical properties. Their surface areas were measured according to the energy conservation law and Stefan-Boltzmann law, manifesting that the surface area of the sheet is around 30 times larger than that of the shrunk yarn. With the measured surface area, the thermionic emission from them was further studied. There is no difference in their work function, emission efficiency, as well as Richardson's emission constant which is approximately equal to the theoretical value of 120.4 A cm^{-2} K^{-2}. The electronic transport properties were studied in low temperature ranging from 3 to 390 K and high temperature around 1100–2300 K. In all the temperature range, there exists a resistance reduction from the MWCNT sheet to the shrunk yarn which was attributed to the increase of intertube crosstalk points between neighboring MWCNTs. It is also found that R decreases with increasing temperature until 1800 K above which R increases due to the electron-phonon scattering at high T.

DOI: 10.1103/PhysRevB.76.045423 PACS number(s): 61.46.−w, 65.80.+n, 78.67.Ch, 73.63.Fg

I. INTRODUCTION

Carbon nanotubes (CNTs) are promising one-dimensional (1D) nanomaterials for their high aspect ratio, excellent electric and thermal conductivities, high tensile strength, and chemical inertness.[1] CNT arrays are self-assembled structures in which high quality CNTs are vertically aligned on substrates.[2–4] In 2002, we have synthesized superaligned multiwalled CNT (MWCNT) arrays in which the CNTs have very clean surfaces and have strong van der Waals interaction with neighboring CNTs.[5,6] The unique property of the superaligned MWCNT array is that continuous MWCNT thin sheets can be directly dry spun from it. The MWCNT sheets are very thin, transparent, and sticky due to a very high specific surface area. Many applications of the sheet have been demonstrated, such as light filament, polarizer, transparent conducting film, polarized light source, etc.[5,7] Recently, we found that the MWCNT sheets will shrink to a tight yarn after passing through volatile solvents.[6] The MWCNTs in shrunk yarns are closely packed, leading to a high tensile strength and reduced specific surface areas. The shrunk yarns have been used as thermionic electron sources[8] and field emission electron sources.[9]

In this paper, we report the comparative studies on the MWCNT sheets before and after shrinking, i.e., the MWCNT sheets and shrunk yarns. It is found that both the thermionic emission properties and the electronic transport properties have been changed dramatically after shrinking. The reason lies in the fact that the specific surface area has been greatly reduced after shrinking. It is well known that the specific surface area of CNTs is much larger than those of general materials for their 1D tube structure and extremely small diameter. The surface area of individual CNT can be estimated from the transmission electron microscopy image of it. Effective surface area of massive CNTs can be obtained from Brunauer-Emmet-Teller (BET) measurement.[10] Here, we introduce another approach for measuring the effective surface areas of MWCNT sheets before and after shrinking. On the basis of the effective surface area measurement, Richardson's constant was determined by thermionic emission, which is nearly equal to the theoretical value of 120.4 A cm^{-2} K^{-2}. The work functions derived from thermionic emission data show no difference for the MWCNT sheet and the shrunk yarn. The effective surface induced electronic transport properties of MWCNTs are also discussed, including I-V characteristics, R reduction from the MWCNT sheet to the shrunk yarn, and R increasing with increasing T at high T.

II. DETERMINATION OF THE EFFECTIVE SURFACE AREA

The superaligned MWCNT arrays were synthesized on 4 in. silicon wafer in a low pressure chemical vapor deposition (LPCVD) system by using 5-nm-thick iron film as catalyst and acetylene as precursor. Details can be found in Ref. 6. Figure 1(a) shows the as-synthesized superaligned MWCNT arrays and the MWCNT sheet drawn from the wafer. Figure 1(b) is the as-fabricated shrunk yarn rolled on a spool with length about tens of meters. Figures 1(c) and 1(d) are scanning electron microscopy (SEM) images of the MWCNT sheet and shrunk yarn showing that the sheet is composed of sparsely aligned CNTs and after shrinking it becomes densely aligned. A 6-mm-wide MWCNT sheet was fixed on two nickel rods with a spacing of 8 mm. Another MWCNT sheet with the same width was pulled through droplets of ethanol, after which it shrank into the MWCNT yarn with the diameter about 20 μm.[6] The shrunk yarn was also mounted on two nickel rods with the same spacing as that for the sheet. Both the MWCNT sheet and the shrunk

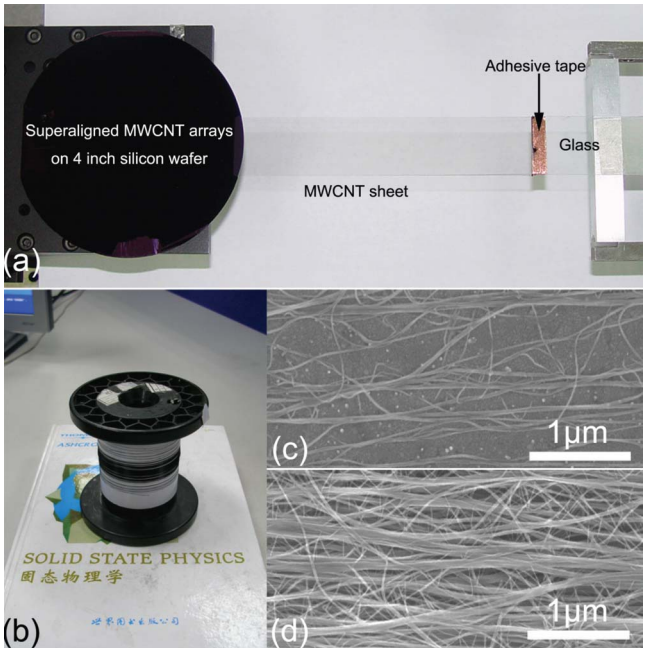

FIG. 1. (Color online) (a) MWCNT sheet drawn from superaligned MWCNT arrays grown on 4 in. silicon wafer by LPCVD method. (b) As-fabricated shrunk yarn rolled on a spool with length about tens of meters. (c) and (d) are SEM images of the MWCNT sheet and the shrunk yarn, respectively.

yarn were heated by a direct current in a vacuum chamber with base pressure about 1×10^{-5} Pa. The spectra of the hot sheet and yarn were recorded by a spectrometer (Konica-Minolta CS-1000). The temperature can be derived by fitting the spectra with blackbody radiation law[8,9,11] and generally the uncertainty of temperature measurement by using this method is less than 1 K. The corresponding voltage U and current I were measured by Keithley 2182 and Keithley 2001, respectively.

The inset of Fig. 2 shows the optical images of the current heated CNT sheet and shrunk yarn. If we consider the energy flows in these two systems, according to the energy conservation law, the power input, which is equal to UI, should be equal to the power dissipated. Generally, there are three ways for energy dissipation: heat conducted to the nickel electrodes, photon radiation, and the electron emission. Since the temperatures are very uniform across the whole sheet or yarn (inset of Fig. 2), the heat transferred to the nickel electrodes can be neglected. The energy loss due to electron emission has been theoretically predicted by Richardson more than 100 years ago.[12] An emitted electron will take away an average energy of $\phi+2k_BT$. Then, the power dissipated due to electron emission is

$$\Phi_{el}=(\phi+2k_BT)AST^2e^{-\phi/k_BT}. \tag{1}$$

The energy loss due to photon emission can be well predicted by the Stefan-Boltzmann law which tells that the total radiant power is proportional to T^4 and can be expressed as

$$\Phi_{ph}=\sigma T^4S, \tag{2}$$

where $\sigma=5.67\times10^{-8}$ W/(m^2 K^4) is the Stefan-Boltzmann constant (we assume emissivity=1), T the Kelvin temperature, and UI the heating power.[13] A rough estimation indicates that, contrary to the field electron emission from CNTs,[14] the energy loss due to electron emission Φ_{el} is negligible compared with that due to photon emission Φ_{ph}. Then, according to the conservation law of energy we have

$$UI\approx\sigma T^4S. \tag{3}$$

Therefore, the heating power UI should be proportional to the thermal radiation σT^4 of the MWCNT sheet and yarn. Figure 2 shows the measured UI plotted against the σT^4 for the CNT sheet and shrunk yarn, respectively. Both can be perfectly fitted by straight lines of which the slopes are the effective surface areas: 1.52×10^{-5} m^2 for the MWCNT sheet and 4.51×10^{-7} m^2 for the MWCNT shrunk yarn. The effective surface of the MWCNT sheet is about 16% of its geometric area, indicating that the MWCNT sheet is composed of sparsely aligned MWCNTs, which can be validated by the SEM images. The measured effective areas of the shrunk yarns are generally larger than but not far from the geometrical sizes because of the nanostructured surfaces. It is difficult to accurately determine the geometrical surfaces of the shrunk yarns because of the somewhat irregular structures.[6] These are the reasons for the larger and divergent Richardson's constants we measured in our previous studies.[8] Note that the effective surface area measured here is not the same as that measured by BET. Here, the effective surface area is the surface area for emitting photons or electrons to the environment, which should be smaller than the surface area measured by BET.

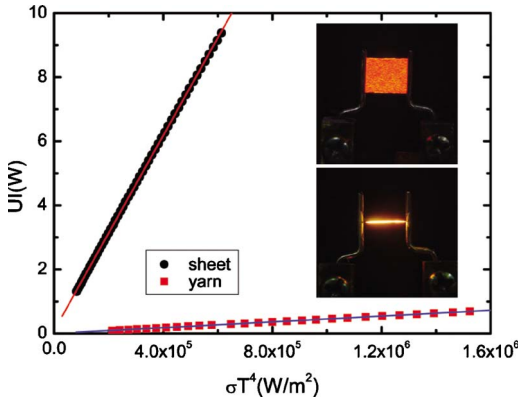

FIG. 2. (Color online) Heating power UI versus σT^4 of both the MWCNT sheet and the yarn. The top right inset is the hot suspended MWCNT sheet heated by a dc source under $\sim1\times10^{-5}$ Pa vacuum and the bottom right inset is the hot shrunk yarn.

III. THERMIONIC EMISSION AND RICHARDSON'S CONSTANT

Recently, we have investigated the thermionic emission from the MWCNT shrunk yarn of which the work function has been determined by using the method proposed by Richardson.[8,15] In that paper, we estimated the surface area by assuming a perfect cylinder surface for the shrunk yarn,

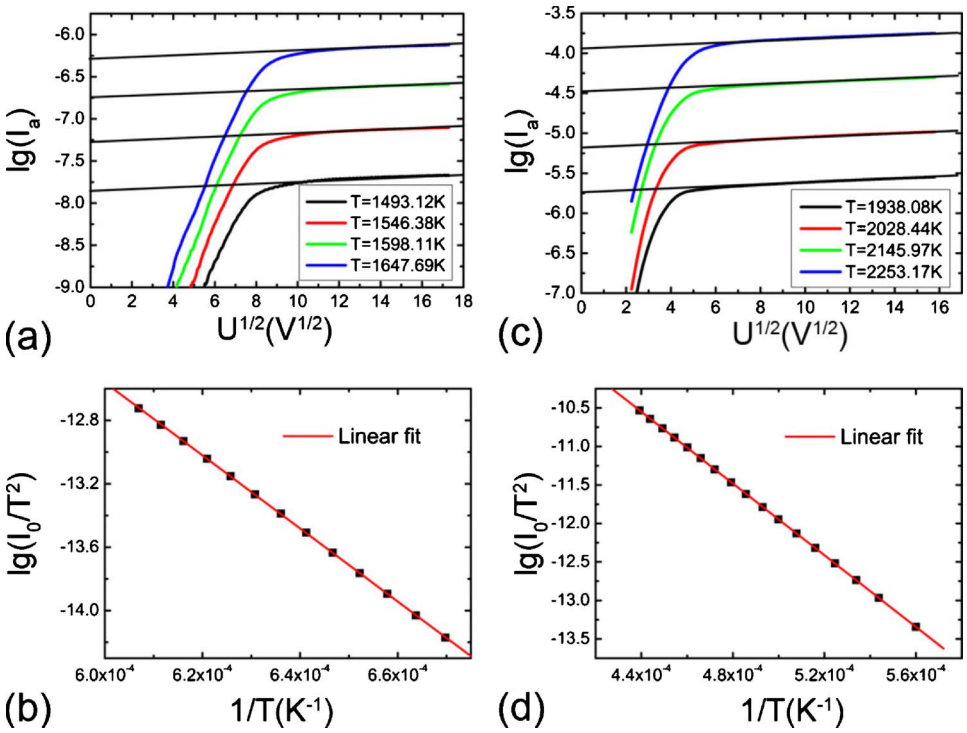

FIG. 3. (Color online) (a) The $\log I_a \sim \sqrt{U}$ curves of the MWCNT sheet. The straight lines represent the results of linearly fitting in accelerating field regime. (b) Experimental data (solid square) and fitted line in $\log(I_0/T^2)$ versus $1/T$ plot of the MWCNT sheet. (c) The $\log I_a \sim \sqrt{U}$ curves of the shrunk yarn. (d) Experimental data (solid square) and fitted line in $\log(I_0/T^2)$ versus $1/T$ plot of the shrunk yarn.

which is smaller than the real surface area of the shrunk yarn. Therefore, Richardson's constant obtained in that paper is larger than the theoretical value. Here, we present our comparative investigations on the thermionic emission properties of both the suspended MWCNT sheets and the corresponding shrunk yarns, aiming at determining the work function and Richardson's constants for both type of materials.

For a thermionic electron source, the emission current depends on the work function, effective surface area, and temperature of the cathode, which follows Richardson's formula:[15]

$$I_0 = AST^2 e^{-\phi/k_B T}, \tag{4}$$

where I_0 is the zero-field emission current, A the Richardson emission constant, S the effective surface area, T the temperature in Kelvin scale, ϕ the work function of cathode, and k_B the Boltzmann constant.

The emission current versus external electric field in the accelerating field region can be expressed as

$$\log I_a \approx \log I_0 + 1.906 \frac{\sqrt{\alpha}}{T} \sqrt{U_a}, \tag{5}$$

where I_a is the current collected by the anode with potential U_a and α is a constant in cm^{-1} determined by the electrode geometry. The temperature T was obtained by fitting the light emission spectra (recorded by Konica Minolta CS-1000S) with blackbody radiation law.[8,11] The corresponding $I_a \sim U_a$ curves of the MWCNT sheets and yarns at various temperatures were simultaneously measured by Keithley 237. Figures 3(a) and 3(c) show typical $\log I_a \sim \sqrt{U}$ curves of the MWCNT sheet and corresponding shrunk yarn. If $\log I_a$ is plotted against $\sqrt{U_a}$, and fitted by a straight line, the intercept on the y axis should be $\log I_0$.

Conducting logarithm operation on both sides of Eq. (4), we have

$$\log\left(\frac{I_0}{T^2}\right) = \log(AS) - 0.4343\frac{\phi}{k_B T}, \tag{6}$$

where S is the emission area. With $\log I_0$ at various temperatures, the work function can be determined from the slope of $\log(I_0/T^2) \sim 1/T$. The measured work functions of these two types of samples are listed in Table I, which are all around 4.6 eV and equal to the work function of the shrunk yarn measured in Ref. 8.

Since the effective surface area has been measured by the aforementioned method, we can also determine Richardson's emission constant from the intercept on the y axis of the $\log(I_0/T^2) \sim 1/T$ plot. The measured Richardson's emission constants for the MWCNT sheets and shrunk yarns are listed in Table I, which are all approximately equal to the theoretical value of 120.4 A cm^{-2} K^{-2}, indicating that the thermi-

TABLE I. The effective surface area (S_{eff}), work function (ϕ), and Richardson's constant (A) of the MWCNT sheets and shrunk yarns.

Sample	S_{eff} (m^2)	ϕ (eV)	A (A cm^{-2} K^{-2})
1_sheet	1.52×10^{-5}	4.57	120
1_yarn	4.51×10^{-7}	4.62	111
2_sheet	7.85×10^{-6}	4.55	125
2_yarn	3.66×10^{-7}	4.60	128
3_sheet	7.20×10^{-6}	4.62	133

onic emission from both the MWCNT sheets and the shrunk yarns follows Richardson's theory very well.

However, it has to be pointed out that the effective surface areas adopted here were assumed to be equal to the surface areas measured according to the Stefan-Boltzmann law, which were the effective surface area for photon emission. This area should be smaller than the surface area measured by the BET method which is based on adsorption measurement. The reason lies in the fact that some inner surfaces can exchange photons and do not contribute to the radiant power. Also, these inner surfaces can exchange electrons; consequently, it is reasonable that the surface area for electron emission is the same as that for photon emission. This assumption is also supported by the fact that the derived Richardson's emission constant is equal to the theoretical value, indicating that the aforementioned method for determining the effective surface area is valid.

From the experimental results listed in Table I, we can see that both the work function and Richardson's emission constant of the MWCNT sheets are the same as those of shrunk yarns. Another important parameter for their application as thermionic cathode is the emission efficiency which is defined as the ratio of the emission current to the input power. For both the MWCNT sheets and the shrunk yarns, the emission efficiency can be written as

$$\eta = \frac{I_0}{UI} = \frac{A}{\sigma}\frac{1}{T^2}e^{-\phi/k_B T}, \tag{7}$$

which is only related with the temperature T. Therefore, the emission efficiency of the MWCNT sheet is the same as that of the shrunk yarn provided that they work at the same temperature. The experimental data of the emission efficiency of both the sheet and the shrunk yarn were plotted in Fig. 4, which fit very well with the theoretical curve [calculated from Eq. (7) by assuming ϕ and A equal to 4.6 eV and 120.4 A cm^{-2} K^{-2}, respectively]. The inset of Fig. 4 is the magnified plot of the emission efficiency data in the green rectangle, distinctly indicating that η is identical for the sheet and the shrunk yarn at the same temperature. To reach the same temperature, however, the MWCNT sheet needs much higher input power dissipated via thermal radiation than the shrunk yarn due to larger surface area. For example, an input power of 9.378 W (I=107.795 mA, U=87.00 V) was needed to heat the MWCNT sheet to 1813.6 K (I_0=1.06 $\times 10^{-5}$ A), but only an input power of 0.292 W (I=21.639 mA, U=13.50 V) was sufficient to heat the shrunk yarn to 1839.1 K (I_0=3.67$\times 10^{-7}$ A). That is to say, at the same temperature the thermionic emission current of the MWCNT sheet is much larger than that of the shrunk yarn for the large effective surface area.

From our experiments, we also found that the maximum temperature that can be reached by the shrunk yarns was much higher than that by sheets. Furthermore, the maximum emission current of the sheet (sample 1_sheet) was about 17.6 μA at 1813.6 K, and that corresponding to the shrunk yarn (sample 1_yarn) was about 230 μA at 2277.0 K. Since the thermionic emission current density exponentially depends on the temperature and linearly depends on the effective surface area, therefore the MWCNT shrunk yarn is a better choice of thermionic electron sources than the MWCNT sheet, even though the effective surface of the MWCNT sheets is much larger than that of the shrunk yarns.

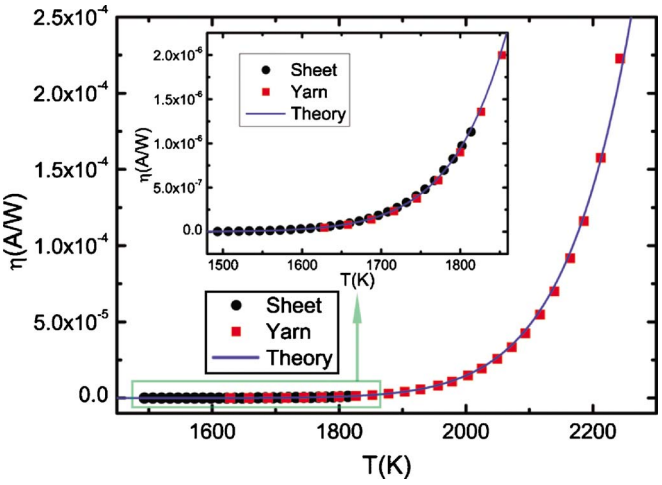

FIG. 4. (Color online) The emission efficiency versus T of both the MWCNT sheet and the shrunk yarn in which the black solid circles are the experiment data for the MWCNT sheet, the red solid squares are the experiment data for the shrunk yarn, and the blue solid line is the theory curve with ϕ=4.6 eV and A =120.4 A cm^{-2} K^{-2}. The inset is the magnified plot of the emission efficiency data in the green rectangle, indicating that η is identical for the sheet and the shrunk yarn working at the same temperature.

Since the work function of the MWCNT yarn is almost the same as that of tungsten (4.54 eV), it is therefore expected that the MWCNT yarn should have the same performance as tungsten hot cathode. Due to the nanostructured surface, the MWCNT yarn has a larger effective surface area as well as higher emission current than tungsten if they work at the same temperature.[8] However, for MWCNT, the maximum working temperature is lower than that for tungsten.

IV. ELECTRONIC TRANSPORT PROPERTIES AND RESISTANCE REDUCTION

The electronic transport properties of the MWCNT sheets and shrunk yarns were also investigated at low temperatures (from 3 to 390 K) and high temperatures (from 1100 to 2300 K). The low temperature electronic transport properties were investigated in a low temperature probe station (LakeShore Cryotronics, Inc.) by using Keithley 4200. The I-V characteristics and the high temperature electronic transport properties were investigated in a vacuum chamber with a base pressure of 1×10^{-5} Pa by using Keithley 237.

The typical I-V curves for the MWCNT sheets and shrunk yarns in vacuum are shown in Fig. 5, which are quite different from each other. The current passing through the MWCNT sheet increased nonlinearly with voltage, indicating that its resistance decreased with voltage. The same behavior has been previously reported by ourselves[5] and Zhang *et al.*[7] For the shrunk yarn, the resistance is much less than that of the sheet, and decreases first with voltage and then increases again. Because the sheet and the yarn can be heated

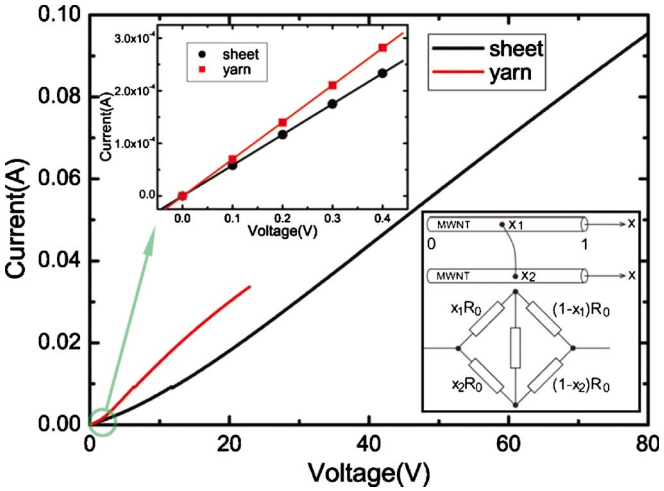

FIG. 5. (Color online) *I-V* characteristics of the suspended MWCNT sheet and the shrunk yarn. The top left inset is the *I-V* curve at low heating power and the bottom right inset is the electric bridge model for the resistance reduction.

by current to high temperatures in vacuum, we attribute these nonlinear behavior to the temperature effect.

If we look at the *I-V* curve near zero bias (top left inset of Fig. 5), which corresponds to the room temperature measurement, it is found that R was lowered from 1714.7±0.2 Ω for the MWCNT sheet to 1420±4 Ω for the shrunk yarn. The resistance reduction appears to be a result of MWCNT bunching. This bunching effect can also be observed if we blow the MWCNT sheet. The MWCNT sheet was first drawn from a superaligned MWCNT array and then directly covered on a glass substrate with the two ends fixed by silver paste as electrical contacts (top left inset of Fig. 6). A bias of 2 V was applied on the two silver paste electrodes and the currents were monitored by Keithley 237. If the MWCNT sheet was blown by air, the continuous sheet will be turned

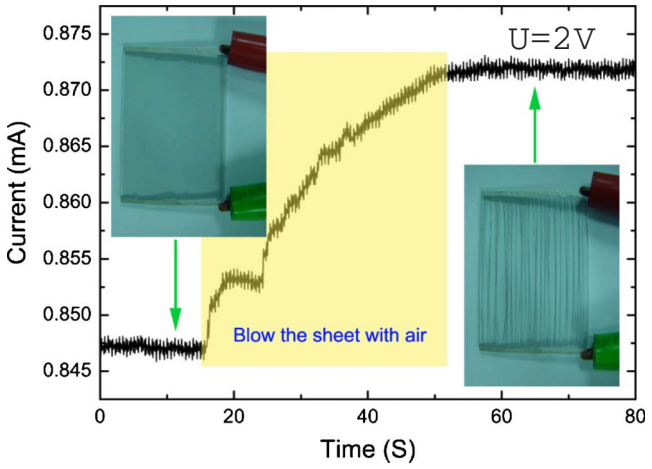

FIG. 6. (Color online) The *in situ* observation of the resistance reduction from the MWCNT sheet to the shrunk yarn. The top left inset is the MWCNT sheet covered on a glass substrate with the two ends fixed by silver paste. The bottom right inset is the morphology of the shrunk yarn after the sheet was blown by air.

into many parallel shrunk yarns (bottom right inset of Fig. 6). During the blowing process, an apparent current jump was observed (Fig. 6), manifesting again the bunching induced resistance reduction.

We then conducted four probe measurement of the resistance of the MWCNT sheet and the shrunk yarn from 3 to 390 K in a low temperature probe station (LakeShore Cryotronics, Inc.). The resistance decreased as the temperature increased. The resistance reduction is obvious for the shrunk yarn in all the temperature range.

The bunching induced resistance reduction can be explained by a simple model. The suspended MWCNT sheet is constructed by joint MWCNTs,[5] and surface reduction from the MWCNT sheet to the shrunk yarn leads to forming a huge amount of intertube contact points. Before forming these intertube contacts, the electric potentials at the intertube contact points are generally different for the neighboring MWCNTs, leading to crosstalk between neighboring nanotubes. To analyze the relation between the increase of contact point and resistance reduction, we established a simple bridge model (bottom right inset of Fig. 5) with one contact point between two same CNTs. The resistance of CNT and the contact resistance are R_0 and R_c, respectively. The analytical solution of the electric bridge can be expressed as

$$R = \frac{R_0}{2}\frac{[(x_1+x_2)-(x_1^2+x_2^2)]R_0+R_c}{(x_1+x_2)\left(1-\frac{x_1+x_2}{2}\right)R_0+R_c} \leqslant \frac{R_0}{2}. \qquad (8)$$

The equality $R=R_0/2$ occurs only when $x_1=x_2$, corresponding to the situation that the contact points have equal electric potential before contacting. In a complex network such as a MWCNT sheet, the potentials are generally different, leading to the resistance reduction. Therefore, the increase of intertube crosstalk might be the reason for the resistance reduction when the MWCNT sheet was shrunk into the yarn.

As shown in Fig. 7(a), R decreases with increasing T and $[R(3\ \mathrm{K})-R(390\ \mathrm{K})]/R(3\ \mathrm{K})$ are 27% for the MWCNT sheet and 31% for the shrunk yarn, respectively. The nonmetallic behavior of the resistance decreasing with temperature for the MWCNT sheet and the shrunk yarn is generally consistent with the model involving electron hopping along thermally activated defect sites along the length of the nanotubes,[16,17] and fluctuation-assisted tunneling through barriers.[18] The sharp decrease in R above 40 K which can be found from Fig. 7(a) agrees well with the results of Skákálová *et al.* and it has been ascribed to the onset of thermally assisted transfer of electrons from the outer shell to the second shell.[19]

$R(T)$ in the range of high temperature is an important property of MWCNT sheets and shrunk yarns for some high temperature applications such as polarized incandescent light source[7] and thermionic electron gun.[8] Here, we derive $R(T)$ from the measured *I-V* curves. Since we have experimentally confirmed the relation $UI \sim \sigma T^4$, the temperature at each point on the *I-V* curve can be determined. Then, the $R(T)$ can be obtained. For the sake of reliability, we only converted the $R(T)$ in the temperature range where we have the experimen-

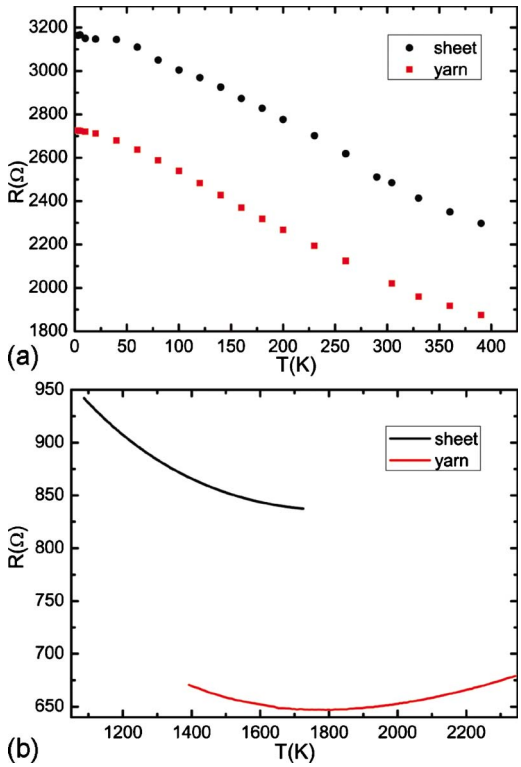

FIG. 7. (Color online) (a) R versus T of the MWCNT sheet and the shrunk yarn measured by four-probe method from 3 to 390 K. R of the shrunk yarn is less than that of the sheet in the full temperature range. (b) $R(T)$ of the sheet and the shrunk yarn at high temperature and R of the shrunk yarn increasing with increasing T after T is higher than 1800 K.

tal data of $UI \sim \sigma T^4$. The converted $R(T)$ of the MWCNT sheet and the shrunk yarn are presented in Fig. 7(b) and both were reproducible. Also, the R reduction from the sheet to the shrunk yarn still exists at high temperature. The MWCNT sheet was prone to be broken at high temperature; therefore, the temperature range of the calibrated $R(T)$ curve of the MWCNT sheet was lower than that of the MWCNT yarn.

From Fig. 7(b), we can see that R of the shrunk yarn first decreases and then increases with increasing T and the turning point is around 1800 K. Several groups have reported similar phenomena of single walled CNTs,[20–22] but here we report that $R(T)$ of the MWCNT system have a crossover point at this high temperature. The expression for R as a function of T is dependent on electron scattering mechanism. Purcell *et al.*[23] assumed that $R(T)=R_0(1-\alpha T)$, where α is the resistance temperature coefficient. Huang *et al.*[24] have made an assumption that R should not decrease indefinitely, and some mechanisms such as electron-phonon scattering[25] can make R increase with T which can be expressed as $R(T)=R_0(1-\alpha T+\beta T^{3/2})$. The third item makes R increase with increasing T at high temperature. Here, we experimentally validate the assumption on the increase of R with increasing T for MWCNTs at high temperature.

V. CONCLUSION

The physical properties of the MWCNT sheets and shrunk yarns have been comparatively studied. Their major differences lie in the surface area and intertube interactions. We have developed an efficient method to measure their surface areas which manifest that the surface area of the sheet is around 30 times larger than that of the shrunk yarn. With the measured surface area, the thermionic emission from them was further investigated. It is found that they both follow Richardson's theory very well. There is no difference in their work function, emission efficiency, as well as Richardson's emission constant which is approximately equal to the theoretical value of 120.4 A cm^{-2} K^{-2}. The electronic transport properties are also investigated in low temperature ranging from 3 to 390 K and high temperature around 1100–2300 K. In all the temperature range, there exists a resistance reduction from the MWCNT sheet to the shrunk yarn which was attributed to the increase of intertube crosstalk points between neighboring MWCNTs. It is also found that R decreases with increasing temperature until 1800 K above which R increases due to the electron-phonon scattering at high T.

ACKNOWLEDGMENTS

We thank Zhaofu Hu and Zhi Zheng for valuable discussions and proofreading. We also acknowledge the financial support from National Basic Research Program of China (2005CB623606) and NSFC (10334060).

*JiangKL@mail.tsinghua.edu.cn
†liuliang@mail.tsinghua.edu.cn

[1] R. Saito, G. Dresselhaus, and M. S. Dresselhaus, *Physical Properties of Carbon Nanotubes* (World Scientific, Singapore, 1998).
[2] W. Z. Li, S. S. Xie, L. X. Qian, B. H. Chang, B. S. Zou, W. Y. Zhou, R. A. Zhao, and G. Wang, Science **274**, 1701 (1996).
[3] Z. F. Ren, Z. P. Huang, J. W. Xu, J. H. Wang, P. Bush, M. P. Siegal, and P. N. Provencio, Science **282**, 1105 (1998).
[4] S. S. Fan, M. G. Chapline, N. R. Franklin, T. W. Tombler, A. M. Cassell, and H. J. Dai, Science **283**, 512 (1999).
[5] K. L. Jiang, Q. Q. Li, and S. S. Fan, Nature (London) **419**, 801 (2002).
[6] X. B. Zhang, K. L. Jiang, C. Feng, P. Liu, L. Zhang, J. Kong, T. H. Zhang, Q. Q. Li, and S. S. Fan, Adv. Mater. (Weinheim, Ger.) **18**, 1505 (2006).
[7] M. Zhang, S. L. Fang, A. A. Zakhidov, S. B. Lee, A. E. Aliev, C. D. Williams, K. R. Atkinson, and R. H. Baughman, Science **309**, 1215 (2005).
[8] P. Liu, Y. Wei, K. L. Jiang, Q. Sun, X. B. Zhang, S. S. Fan, S. F. Zhang, C. G. Ning, and J. K. Deng, Phys. Rev. B **73**, 235412 (2006).
[9] Y. Wei, D. Weng, Y. C. Yang, X. B. Zhang, K. L. Jiang, L. Liu,

and S. S. Fan, Appl. Phys. Lett. **89**, 063101 (2006).
[10] H. Gao, X. B. Wu, J. T. Li, G. T. Wu, J. Y. Lin, K. Wu, and D. S. Xu, Appl. Phys. Lett. **83**, 3389 (2003).
[11] P. Li, K. L. Jiang, M. Liu, Q. Q. Li, and S. S. Fan, Appl. Phys. Lett. **82**, 1763 (2003).
[12] O. W. Richardson, Philos. Trans. R. Soc. London, Ser. A **201**, 497 (1903).
[13] W. Elenbaas, *Light Sources* (Crane, Russak, New York, 1972).
[14] W. Wei, Y. Liu, Y. Wei, K. L. Jiang, L. M. Peng, and S. S. Fan, Nano Lett. **7**, 64 (2007).
[15] O. W. Richardson, *The Emission of Electricity from Hot Bodies*, 2nd ed. (Longmans, Green, London, 1921).
[16] T. W. Ebbesen, H. J. Lezec, H. Hiura, J. W. Bennett, H. F. Ghaemi, and T. Thio, Nature (London) **382**, 54 (1996).
[17] S. B. Lee, K. B. K. Teo, M. Chhowalla, D. G. Hasko, G. A. J. Amaratunga, W. I. Milne, and H. Ahmed, Microelectron. Eng. **61-2**, 475 (2002).
[18] V. Skákálová, A. B. Kaiser, U. Dettlaff-Weglikowska, K. Hrnčariková, and S. Roth, J. Phys. Chem. B **109**, 7174 (2005).
[19] V. Skákálová, A. B. Kaiser, Y. S. Woo, and S. Roth, Phys. Rev. B **74**, 085403 (2006).
[20] J. E. Fischer, H. Dai, A. Thess, R. Lee, N. M. Hanjani, D. L. Dehaas, and R. E. Smalley, Phys. Rev. B **55**, R4921 (1997).
[21] O. Hilt, H. B. Brom, and M. Ahlskog, Phys. Rev. B **61**, R5129 (2000).
[22] M. S. Fuhrer, W. Holmes, P. L. Richards, P. Delaney, S. G. Louie, and A. Zettl, Synth. Met. **103**, 2529 (1999).
[23] S. T. Purcell, P. Vincent, C. Journet, and V. Thien Binh, Phys. Rev. Lett. **88**, 105502 (2002).
[24] N. Y. Huang, J. C. She, J. Chen, S. Z. Deng, N. S. Xu, H. Bishop, S. E. Huq, L. Wang, D. Y. Zhong, E. G. Wang, and D. M. Chen, Phys. Rev. Lett. **93**, 075501 (2004).
[25] E. Pop, D. Mann, J. Cao, Q. Wang, K. Goodson, and H. J. Dai, Phys. Rev. Lett. **95**, 155505 (2005).